Research Article

Nano Biomed Eng

Morphological, Optical, ElectricalCharacterizations and Anti-Escherichia coli Bacterial Efficiency (AECBE) of PVA/PAAm/PEO Polymer Blend Doped with Silver NPs

Karar Abdali[1], Khalid Haneen Abass[2]✉, Ehssan Al-Bermany[2], Enas M. Al-robayi[3], Ashraq M. Kadim[4]

[1]Ministry of Education, Baghdad, Iraq.
[2]Physics Department, College of Education for Pure Sciences, University of Babylon, Iraq.
[3]Physics Department, College of Science, University of Babylon, Iraq.
[4]Medical Physics Department, Hilla University College, Iraq.

✉ Corresponding authors. E-mail: pure.khalid.haneen@uobabylon.edu.iq

Received: Nov. 8, 2021; **Accepted:** Oct. 18 2022; **Published:** Nov. 23, 2022

Citation: KararAbdali, Khalid HaneenAbass, Ehssan Al-Bermany, Enas M. Al-robayi, and Ashraq M. Kadim, Morphological, Optical, Electrical Characterizations and Anti-Escherichia coli Bacterial Efficiency (AECBE) of PVA/PAAm/PEO Polymer Blend Doped with Silver NPs. *Nano Biomed. Eng.*, 2022, 14(2): 114-122.

DOI: 10.5101/nbe.v14i2.p114-122.

Abstract

In the current research, silver nanoparticles (AgNPs) were mixed with a polymer blend to enhance their optical and electrical properties and antibacterial efficiency. A novel approach via introducing AgNPs into the polymer blend could improve the physical and antibacterial characteristics of the nanocomposites (NCs). In the loading process, two different amounts of AgNPs were respectively encapsulated with polyvinyl alcohol (PVA), polyacrylamide (PAAm) and polyethylene oxide (PEO) polymeric blend via casting method. The prepared films were characterized by X-ray, optical microscope (OM), scanning electron microscopy (SEM), Fourier transformation infrared (FTIR) and UV/Visible. The OM and SEM images showed that the AgNPs were well diffused inside the polymer blend with some weak aggregations. The optical properties were enhanced after doping. The NCs films absorbed UV-ray at (λ=220 nm). The indirect energy gap decreased after loading from 3.80 to 3.10 eV but the direct energy gap decreased from 4.25 to 3.75 eV. The AC electrical properties were studied in the frequency range between 100 Hz to 5 MHz. The dielectric constant and loss of NC films were decreased with the increase of AgNPs, while the electrical conductivity increased. The inhibition zone diameters of Escherichia coli bacteria increased with the increasing of AgNPs contents.

Keywords: PEO, Silver NPs, AC conductivity, Antibacterial

Introduction

AgNPs has been famous as an antibacterial (ANB) factor for centuries. It has been reported that AgNPs and hybrid Ag NCs are efficient biocides versus various types of fungi, bacteria, and viruses via releasing Ag^+ which can inactivate the bacteria cells through damaging the membrane of cell and replication capability of DNA. Nanomaterials and nanotechnology are of much interest for the development of new ANB approaches, based on either novel biomaterials or on enhancing the biological features of the existing ones [1]. Currently, in a sustainable and eco-friendly driven approach, many studies are directed to design both clinically and environmentally safe nanomaterials for ANB applications. Hybrid polymer NCs are a novel type of material with unique physical and chemical properties. These NCs have recently attracted serious research attention due to their tangible potential for a wide range of applications in environmental

solutions and the resolution of many environmental aspects [1]. The dynamic interface between NPs and polymer basis is the most challenging aspect of NCs [2]. Hybrid polymer NCs bring a novelty of several type of materials with unique physical and chemical properties [1, 2]. These NPs have nano dimensions, large specific area and energy sites in the surfaces are formed that underline the importance of polymer-nanoparticles interactions [3-5]. Through, numerous studies have offering that AgNPs with small average grain size are eligible for the ANB control system, due to the strong cell permeation and high fixed surface area [6, 7]. However, there are two significant challenges for AgNPs in utilizations: NPs agglomeration and nanomaterial recapture, which would lead to missing the ANB efficiency of AgNPs [8]. The AgNPs doped polymeric blends have been studied by several researchers [9-18]. PVA is water soluble polymer (WSP) from vinyl polymer classes. PVA is derived from poly(vinyl acetate). It's usually used in coatings for photographic films, cosmetics, antibacterial and medical applications. It has a different viscosity grades [19-22]. PAAm is another WSP, has a wide ranges of industrial and medical applications. The major applications of PAAm are flocculants in water treatment, paper manufacture, mining, oil recovery, absorbents and gels for electrophoresis. The applications of PAAm are useful as a result of mechanical properties of vulnerable tensile strength [23-25]. It has a great ability to fool water and produce colloidal solution which makes it a good filter for forming gel polymer electrolyte. The electrical conductivity of PAAm is greater than (10^{-2} $S{\cdot}cm^{-1}$) at room temperature (RT) [26, 27]. PEO has a major applications in flocculants of water treatment, manufacture of papers, mining, oil recapture, absorbents and electrophoresis gels [28]. The optical properties of AgNPs are highly conditioned on the nanoparticle diameters [29]. The smaller diameter of Ag almost absorbs light and has peaks around 400 nm then, the dispersion extends to red-shifting [30]. The solution casting way is established on the Stokes' law principle. In this way, the pre-polymer and polymer are equally incorporated and make soluble in the appropriate solution. The polymer being the basis phase dissolved easily soluble in the solution, while the NPs scattered in different solution or same solution [30]. The essential aim of this research is to study the effect of AgNPs on structural, optical, electrical characteristics and ANB efficiency of PVA/PAAm/PEO polymer blend.

Experimental

Materials

PVA (Mw ~18000 and 99% assay purity) was purchased from (DIDACTIC), PAAm (Mw over 5000k and 99.9% purity) was purchased from (CDH), PEO (Mw ~6k and 99.8% purity) was supplied from (Reagent World) and AgNPs was purchased from (Sky Spring Nanomaterials, Inc.) with an average grain size about (20-30) nm and assay purity of (99.95%).

Syntheses of NCs

The (60:20:20) wt./wt.% of PVA, PAAm and PEO was separately dissolved in (35 mL) distilled water as an polymer blend. The mixture was thereafter stirred for 2 hrs. via a magnetic stirrer for 60 °C. The polymer blend solution was casted and left to dry for a week via casting method. In the doping process 0, 0.02 and 0.04 AgNPs were respectively added to the polymer blend solution, as offered in Table 1. To homogenize these PNCs, stirring was made for 45 min. The thicknesses of PNCs films were computed by digital micrometer to be between 0.080 and 0.095 cm.

Table 1 PVA/PAAm/PEO)/AgNPs weight percentages

PVA 60 w.t.%	PAAm 20 w.t.%	PEO 20 w.t.%	AgNPs w.t.%
0.600	0.200	0.200	0.00
0.588	0.196	0.196	0.02
0.576	0.192	0.192	0.04

Characterization

The X-ray diffractometer type pert high score (2008) was used to investigate the crystal structure nature. A Nikon Olympus (73346) was used to show the OPM images. The chemical bonds were investigated by Bruker (vertex 701) spectrophotometer. The ultra-violet/visible properties were studied by double beam Shimadzu (1800) spectrometer. The AC electrical characteristics were measured by LCR meter, Hi TESTER, HIOKI (3532-50).

Results and Discussion

X-ray diffraction

Figure 1 offers the X-ray diffraction peaks of PVA/PAAm/PEO polymer blend without and with different AgNPs contents. The X-ray diffraction chart of PVA/PAAm/PEO shows just one peak refer to the semi crystalline nature of polymer blend at ($2\theta = 20°$). The AgNPs showed a significant decrease in the sharpness

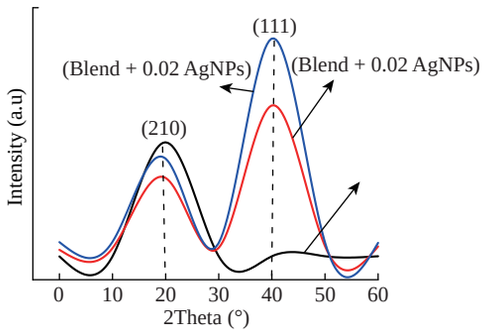

Fig. 1 The XRD pattern of PVA/PAAm/PEO and AgNPs doped PVA/PAAm/PEO.

of peak of PVA/PAAm/PEO. This is may be due to the interaction which occurred between them. The AgNPs appear at 2θ = 40°. The X-ray diffraction peaks show that the crystallinity of polymer blend was enhanced after doping. The AgNPs doped PVA/PAAm/PEO has face center cubic structure.

OPM and SEM images

Figures 2 and 3 represent the OPM and SEM images of AgNPs doped (PVA/PAAm/PEO) at magnification power of 100X. From Fig. 2, part-A shows that the polymer blends have acceptable and homogenous dissolving, while the parts B and C in same Figure show the diffusion of AgNPs on the surface of blends. There is some weak agglomerations appeared in the part B and C, due to the interactions among AgNPs. The morphology and surface fraction of the NCs films were also investigated using the SEM, as shown in Fig. 3. Figure 3(A) displays a SEM image of a homogeneous polymer surface with uniform morphology. The changes of the composition of the surface were happened by AgNPs. This could indicate that the occurrence of a homogeneous growth mechanism without aggregations, as shown in Fig. 3(B). In SEM images, the size of AgNPs was measured on the surface of NCs. The particle sizes of AgNPs were ranged in nanometer dimensions.

FTIR spectrums

Figure 4 shows the FTIR spectrums of PVA/PAAm/PEO after and before loaded with AgNPs in the wavenumber range between 4000-400 cm^{-1}. From the Figure, can be notice that the functional groups appear as, the alcohol/phenol O-H stretch appeared in (3274.27 cm^{-1}), vinyl ether C-O stretching appeared in (1242.31 cm^{-1}), aromatic C-H bending appeared in (695.68 cm^{-1}) and primary alcohol C-O stretching appeaed in (1085.39 cm^{-1}). These peaks referred to the interfacial physical interactions were happened among the mixed materials. The intractions created a novel physical characteristics [31].

Optical properties

The optical properties of PVA/PAAm/PEO blend

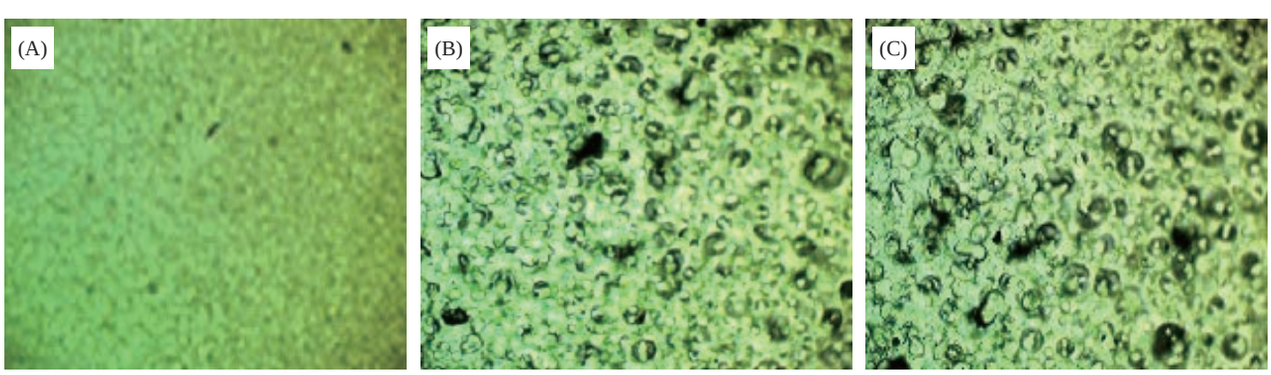

Fig. 2 Photomicrograph images (100X) ofNCs: **(A)** PVA/PAAm/PEO, **(B)** PVA/PAAm/PEO:0.02w.t.% AgNPs, **(C)** PVA/PAAm/PEO:0.04w.t.% AgNPs.

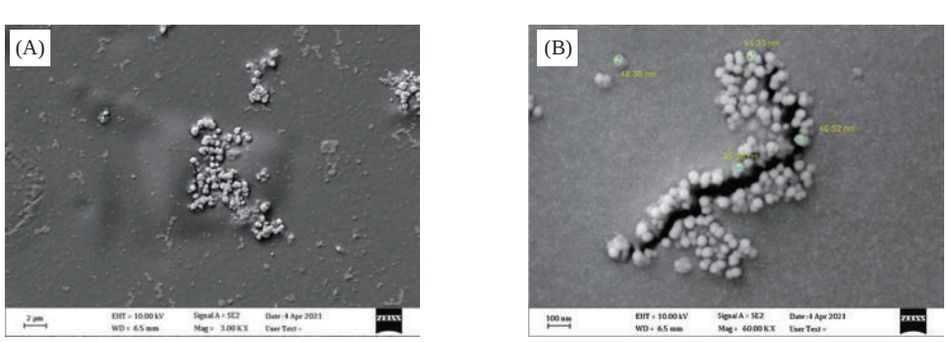

Fig. 3 SEM photomicrographs of **(A)** PVA/PAAm/PEO:0.02w.t.% AgNPs and **(B)** PVA/PAAm/PEO:0.04w.t.% AgNPs.

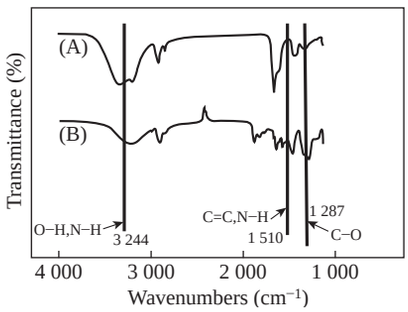

Fig. 4 FTIR spectrum of **(A)** PVA/PAAm/PEO and **(B)** (PVA/PAAm/PEO)/AgNPs.

and its additives with (0, 0.02 and 0.04) w.t.% from AgNPs were studied in the wavelength range between 190 to 1100 nm. The absorption spectra of PVA/PAAm/PEO polymer blend before and after adding AgNPs as a function of wavelengths were presented in Fig. 5 part A. From the figure, noticed that the absorbance spectrum of the prepared films has a maximum wavelength (λ_{max}) in the absorption edge of (200 nm). This absorbance spectrum has a low values in the visible and near IR region, this is because the incident photons do not have enough energy to interact with atoms at a high wavelength and thus transmitted. At low wavelength values, There is an interactions happened between the incident photon and the blend therefore, the absorbance increased [32]. The loading of AgNPs to the polymeric blend clearly enhanced the optical absorbance spectrum, this is maybe because the homogeneous diffusion of AgNPs in the polymer blends [33]. The transmittance spectrums were offered in part B of the same figure. The transmittance values were decreased with the increasing of wavelength. The part C in the same Figure represents the reflectance spectrum. The reflectance values increased with the increasing of AgNPs, but decreased with the wavelengths. This is due to the increasing of density. The refractive index values were calculated by [34] :

$$n = \frac{1+\sqrt{R}}{1-\sqrt{R}} \quad (1)$$

The absorption coefficient (α) values decreased with the increasing of wavelength for prepared films. The (α) of the NCs was calculated by [35]:

$$\alpha = (2.303A)/t \quad (2)$$

The extinction coefficient (k) of nanocomposite has been determined from [36]:

$$k = \alpha\lambda/4\pi \quad (3)$$

In general, we can observe that (k) increase with the increasing of AgNPs for prepared films. Figure 6

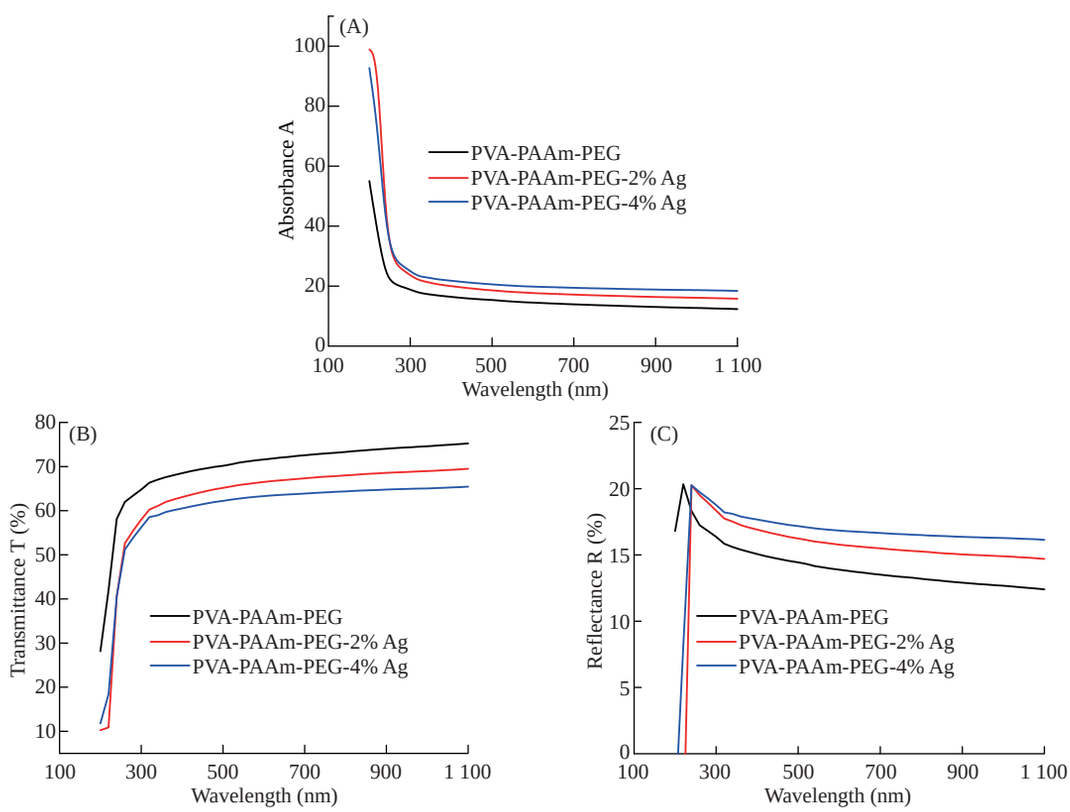

Fig. 5 (A) Absorbance vs. wavelength of (PVA/PAAm/PEO)/Ag, **(B)** Transmittance vs. wavelength of (PVA/PAAm/PEO)/Ag and **(C)** Reflectance vs. wavelength of (PVA/PAAm/PEO)/Ag.

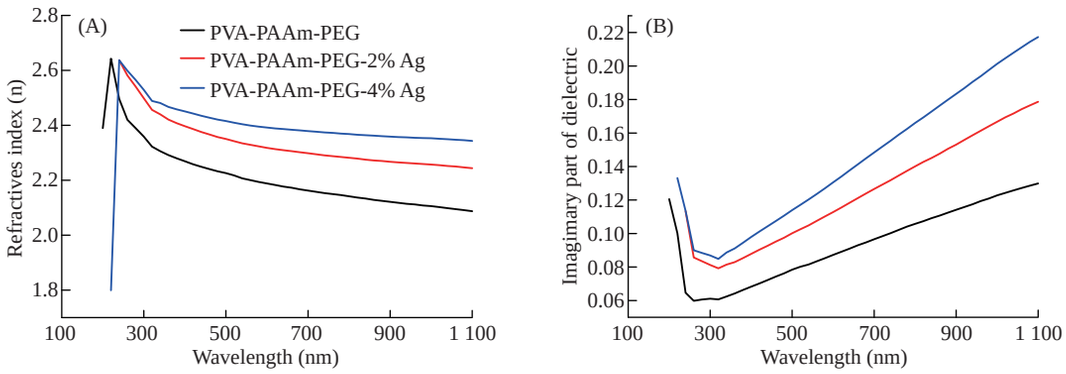

Fig. 6 The refractive index vs. wavelength of NCs films, **(A)** Real part of RI and **(B)** Imaginary part of RI.

shows that the (n and k) of (PVA/PAAm/PEO) with different weight percentage of AgNPs. The (α) values increased with the increasing of AgNPs and energy (hf) as shown in Fig. 7. The values of absorption coefficient were less than (10^4 cm^{-1}), This induces a rise in the likelihood of indirect transitions.

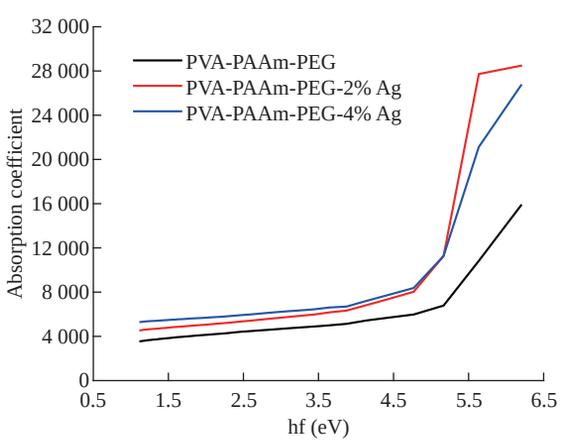

Fig. 7 The absorption coefficient spectrum vs. wavelength of (PVA/PAAm/PEO)/Ag NCs.

The indirect and direct optical energy gap of (PVA/PAAm/PEO)/Ag NCs films were determined by Tauc model [36]:

$$\alpha h\upsilon \approx B(h\upsilon - E_g)^n \quad (4)$$

where (B) is a constant, (n) is a transition sort. The indirect and direct optical energy gaps were offered in Fig. 8. The extrapolation straight line of photon energy at zero $(\alpha h\nu)^{1/2}$ and $(\alpha h\nu)^2$ respectively represent E_g. The decreasing of energy gap values with increasing of AgNPs illustrate the films were semiconductors.

Electrical properties

The dielectric constant (έ) of NCs was defined by [37]:

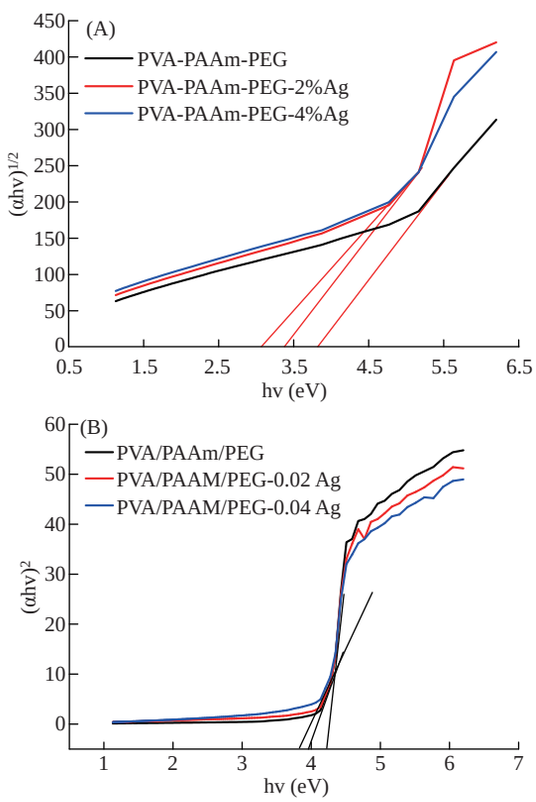

Fig. 8 Tauc plot for **(A)** indirect and **(B)** direct optical energy gap.

$$\acute{\varepsilon} = C_p/C_o \quad (5)$$

where C_p and C_o are parallel and vacuum capacitance.

The dielectric loss (ε″) was given by [37]:

$$\varepsilon'' = \acute{\varepsilon}D \quad (6)$$

where D is dispersion coefficient of NCs.

Figures 9 and 10 show that the variations of dielectric constant and dielectric loss with frequency (f) at RT. From these figures, it is obvious that both dielectric constant and dielectric loss have high values at lower frequency, due to the nature that dipole moments have ample time in these zones to order

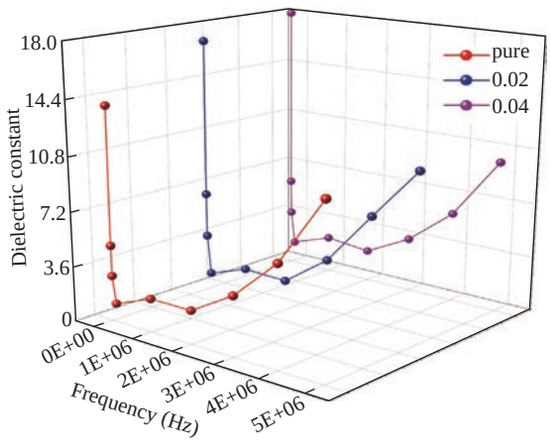

Fig. 9 Dielectric constant vs. frequency of (PVA/PAAm/PEO)/Ag NCs.

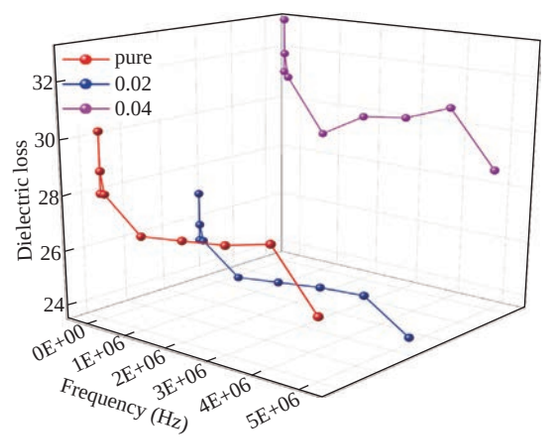

Fig. 10 Dielectric loss vs. frequency of (PVA/PAAm/PEO)/Ag NCs.

themselves in the direction of the applied electric field. In addition, charge carriers are accumulated in the electrode and electrolyte mode due to space charge polarization. The electrode and electrolyte moderator accumulate charge carriers. The dielectric constant and dielectric loss decrease monotonically and reach constant value as the frequency increases. This change in the dielectric parameter relates to the fact that the frequency increases the decreases in the polarization of the space charge and that more ions cannot be spread in the direction of the applied electric field because the dielectric properties are less involved in the charge carriers. The non-Debye sorting behavior of polymer electrolytes is emphasized by this update. The dipole moments are therefore unable to follow up the field differentiation at higher frequencies due to defective time [38]. The dielectric constant and dielectric loss values decreased with the increasing of AgNPs. This is may be because the increasing of electrical conductivity due to the increasing of charge carriers [39, 40].

The electrical conductivity was computed by [41]:

$$\sigma_{A.C} = \omega \varepsilon'' \varepsilon_o \quad (7)$$

where ω is the angular frequency.

Figure 11 shows the electrical conductivity variations of PVA/PAAm/PEO)/Ag NCs with the frequency. The figure demonstrates that this activity can be assigned to the interfacial polarization of the A.C electrical conductivity that increases as the frequency rises. As Ag NPs increase, electrical conductivity increases, which is also due to an increase in the density of the charge carrier in the polymer blend [41].

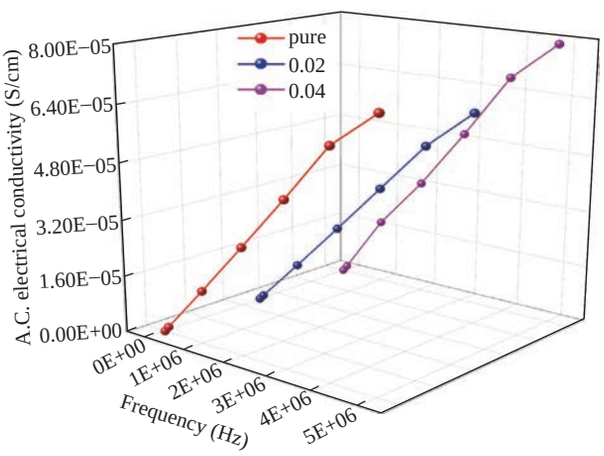

Fig. 11 A.C. electrical conductivity vs. frequency of (PVA/PAAm/PEO)/Ag NCs.

Antibacterial tests

Gram-negative (G−) bacterial progeny Escherichia coli was select as the sample organisms for estimating AECBE of the (PVA/PAAm/PEO)/Ag NCs. The growth of bacterial kinetics of (PVA/PAAm/PEO)/Ag NCs with various AgNPs doping was observed in 5 mL LB soup. As offering in Figs. 12 and 13, a growth retard was appeared versus Escherichia coli. The kinetics of growth was investigated based on the magnitude of optical densities at 500 nm and the result finds that the growth retard follows the order as (matrix/0 Ag) < (matrix/0.02 Ag) < (matrix/0.04 Ag)< (matrix/0.06 Ag). Thus, the doping of AgNPs in the NCs is a crucial factor for AECBE [42, 43]. The AECBE of the films was tested to be applied to the uses as a new characteristic and to be obeyed by other applications. Oxidative stress reasoned by ROS may be the key mechanism which caused the NPs to be AECBE NCs. ROS reflects radicals such as super oxide radicals (O_2), hydroxyl radicals (-OH) and hydrogen peroxide (H_2O_2), and single oxygen (O) could be the reason which the DNA and bacteria's protein were

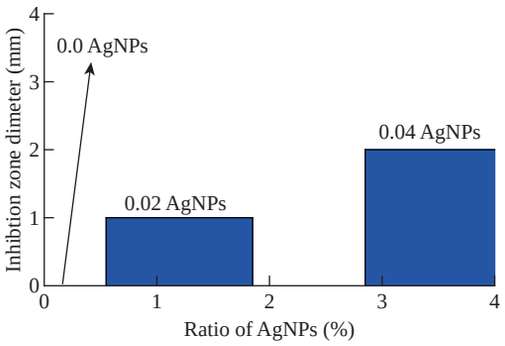

Fig. 12 The inhibition zone diameter of E. coli vs. AgNPs doped PVA/PAAm/PEO weight percentage.

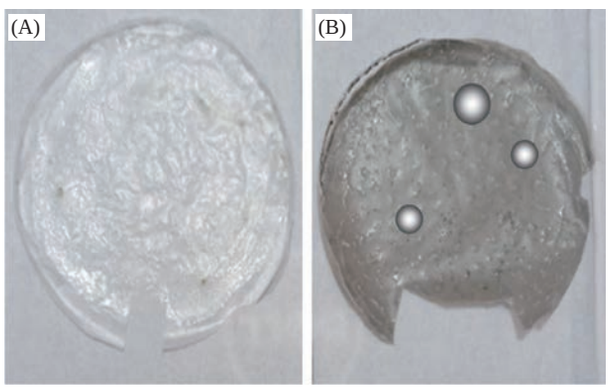

Fig. 13 The activity of NCs films against E. coli bacteria.

inhibited. The current AgNPs could have created ROS, leading to the inhibition of most pathogenic bacteria [18, 43]. The results were compared with [44-50].

Conclusions

The PVA/PAAm/PEO polymer blend without and with AgNPs was successfully prepared by the casting method. The X-ray diffraction peaks appeared a semi-crystalline nature of polymer blend. The crystal structure of AgNPs doped polymer blend was FCC. The images of OPM and SEM showed that the AgNPs were well diffused inside the blend with some weak agglomerations. The optical coefficients increased with the increasing of AgNPs and wavelength except for the transmittance spectrum and optical energy gap. The absorption coefficient edges decreased with the increase of AgNPs and energy. The indirect optical energy gap values decreased from 3.80 to 3.10 eV, but the direct decreased from 4.25 to 3.75 eV. The dielectric constant and loss decreased with the increasing of frequency. The AC electrical conductivity increased with the increasing of AgNPs and frequency. The inhibition zone diameters of Escherichia coli bacteria clearly increased after loading.

Conflict of Interests

The authors declare that no competing interest exists.

References

[1] K. Woo, C. Hye, W. Ki, S. Shin, H. So, H. Yongm. Antibacterial activity and mechanism of action of the silver ion in Staphylococcus aureus and Escherichia coli. *Applied and Environmental Microbiology*. 2008, 74(7): 217-2178.

[2] Q. Feng, J. Wu, G. Chen, F. Cui, T. Kim, J. Kim. A mechanistic study of the antibacterial effect of silver ions on Escherichia coli and Staphylococcus aureus. *Journal of Biomedical Materials Research*. 2000, 52(4): 662-668.

[3] A. Kumar, P. Vemula, P. Ajayan, G. John. Silvernanoparticle-embedded antimicrobial paints based on vegetable oil. *Nature Materials*. 2008, 7(3): 236-241.

[4] V. Craver, J. Smith. Sustainable colloidalsilver-impregnated ceramic filter for point-of-use water treatment. *Environmental Science and Technology*. 2008, 42(3): 927-933.

[5] S. Pal, E. Yoon, Y. Tak, E. Choi, J. Song. Synthesis of highly antibacterial nanocrystalline trivalent silver polydiguanide. *Journal of the American Chemical Society*. 2009, 131(44): 16147-16155.

[6] C. Jones, E. Hoek. A review of the antibacterial effects of silver nanomaterials and potential implications for human health and the environment. *Journal of Nanoparticle Research*. 2010, 12(5): 1531-1551.

[7] J. Morones, J. Elechiguerra, A. Camacho, K. Holt, J. Kouri, J. Ramírez, M. Yacaman. The bactericidal effect of silver nanoparticles. *Nanotechnology*. 2005, 16(10): 2346-2353.

[8] H. Kong, J. Jang. Antibacterial properties of novel poly(methyl methacrylate) nanofiber containing silver nanoparticles. *Langmuir*. 2008, 24(5): 2051-2056.

[9] M. Zainy, N. Huang, S. Kumar, H. Lim, C. Chia, I. Harrison. Simple and scalable preparation of reduced graphene oxide-silver nanocomposites via rapid thermal treatment. *Materials Letters*. 2012, 89: 180-183.

[10] L. Liu, J. Liu, Y. Wang, X. Yan, D. Sun. Facile synthesis of monodispersed silver nanoparticles on graphene oxide sheets with enhanced antibacterial activity. *New Journal of Chemistry*. 2011, 35(7): 1418-1423.

[11] S. Liu, J. Tian, L. Wang, H. Li, Y. Zhang, X. Sun. Stable aqueous dispersion of graphene nanosheets: noncovalent functionalization by a polymeric reducing agent and their subsequent decoration with Ag nanoparticles for enzymeless hydrogen peroxide detection. *Macromolecules*. 2010, 43(23): 10078-10083.

[12] S. Liu, J. Tian, L. Wang, and X. Sun. A method for the production of reduced graphene oxide using benzylamine as a reducing and stabilizing agent and its subsequent decoration with Ag nanoparticles for enzymeless hydrogen peroxide detection. *Carbon*. 2011, 49(10): 3158–3164.

[13] Q. Li, X. Qin, Y. Luo, W. Lu. One-pot synthesis of Ag nanoparticles/reduced graphene oxide nanocomposites and their application for nonenzymatic H_2O_2 detection. *Electrochimica Acta*. 2012, 83: 283-287.

[14] T. Wu, S. Liu, Y. Luo, W. Lu, L. Wang, X. Sun. Surface

plasmon resonance-induced visible light photocatalytic reduction of graphene oxide: using Ag nanoparticles as a plasmonic photocatalyst. *Nanoscale*. 2011, 3(5): 2142-2144.

[15] J. Shen, M. Shi, N. Li, B. Yan, H. Ma, Y. Hu, M. Ye. Facile synthesis and application of Ag-chemically converted graphene nanocomposite. *Nano Research*. 2010, 3(5): 339-349.

[16] M. Das, R. Sarma, R. Saikia, V. Kale, M. Shelke, P. Sengupta. Synthesis of silver nanoparticles in an aqueous suspension of graphene oxide sheets and its antimicrobial activity. *Colloids and Surfaces B: Biointerfaces*. 2011, 83(1): 16-22.

[17] J. Ma, J. Zhang, Z. Xiong, Y. Yong, X. S. Zhao. Preparation, characterization and antibacterial properties of silver-modified graphene oxide. *Journal of Materials Chemistry*. 2011, 21(10): 3350-3352.

[18] L. Huang, H. Yang, Y. Zhang, W. Xiao. Study on synthesis and antibacterial properties of Ag NPs/GO nanocomposites. *Journal of Nanomaterial*. 2016: 1-9.

[19] J. Mark. Polymer Data Handbook. New York: Oxford University Press. 1999: 2.

[20] Latif D., Chiad S., Erhayief M., Abass K., Habubi N., Hussin H (2018) Effects of $FeCl_3$ additives on optical parameters of PVA. Journal of Physics: Conference Series. 1003.

[21] Al-Jamal A., HadiM., Hamood J., Abass K. Particle size effect of Sn on structure and optical properties of PVA-PEO blend. Proceedings - International Conference on Developments in Systems Engineering. 2019: 736-740.

[22] Sharba K., Alkelaby A., Sakhil D., Abass K., Habubi N., Chiad S. Enhancement of Urbach energy and dispersion parameters of polyvinyl alcohol with Kaolin additive. *Neuro Quantology*. 2020, 18(3): 66-73.

[23] N. Syla, F. Aliaj. Swelling and Mechanical Properties of Polyacrylamide Based Hydrogels Prepared by Radiation Induced Polymerization. *Journal of Engineering and Applied Sciences*. 2018, 13(17): 7205-7209.

[24] Al-Khalaf A., Abdali K., Mousa A., Zghair M. Preparation and structural properties of liquid crystalline materials and its transition metals complexes. *Asian Journal of Chemistry*. 2019, 31(2): 393-395.

[25] Khalid H., H. Anas. Reduction of Energy Gap in ZrO_2 Nanoparticles on Structural and Optical Properties of Casted PVA–PAAm Blend. *Journal of Green Engineering*. 2020, 10(7): 4166-4176.

[26] P. Verma, P. Sardar, S. Ghosh, M. Biswas. Conducting Nanocomposites of Polyacrylamide with Acetylene Black and Polyaniline. *Polymer Composites*. 2009, 30(4): 490-496.

[27] A. Jenkins. Polymer Science, A material Science Handbook. University of Sussex, North Holland Publishing Co. 1972: 2.

[28] Bailey, Koleske. Poly(Ehtylene Oxide). Academic Press, New York, 1976.

[29] Al-Zuhairi, A., Allw, A., Abdali K., Rasool S., Mousa A. Synthesis of hyperbranched polymers and study of its optical properties. *Journal of Engineering and Applied Sciences*. 2017, 12(6): 7800-7804.

[30] Karar Abdali. Structural, Morphological, and Gamma Ray Shielding (GRS) Characterization of HVCMC/PVP/PEG Polymer Blend Encapsulated with Silicon Dioxide Nanoparticles. *Silicon*. 2022, 14(1): 6-10. https://doi.org/10.1007/s12633-022-01678-8.

[31] B. Max, W. Emil. Principles of Optics. 7th expanded ed., CUP Archive. 1999.

[32] Wu Y, Yu C, Xing M, Wang L, Guan G. Surface modification of polyvinyl alcohol (PVA)/polyacrylamide (PAAm) hydrogels with polydopamine and REDV for improved applicability. *Journal of Biomedical Materials Research*. 2019, 1081: 1-11.

[33] K. Abdali, Lamis F. Alhak A., Abdulazeez O., Ali A. Enhancing Some Physical Properties of Cosmetic Face Powders. *Journal of Global Pharma Technology*. 2018, 10(3): 75-78.

[34] J. Jeevanandam, A. Barhoum, Y. Chan, A. Dufresne, M. Danquah. Review on nanoparticles and nanostructured materials: history, sources, toxicity and regulations. *Beilstein J. Nanotechnol*. 2018, 9: 1050-1074.

[35] Karar Abdali. Enhancement of some physical properties of polyethylene glycol by adding some polymeric cellulose derivatives and its applications. Ph.D. thesis, College of Science, Babylon University. Iraq. 2015.

[36] J. Carter. Cosmic Creation and Evolution of Matter and Energy. 2nd ed. USA. 2019.

[37] N. Mott, R. Gurney. Electronic Processes in Ionic Crystals. Oxford Univ. Press, London. 1940.

[38] H. Güllü, D. Yıldız. Frequency Dependent Dielectric Properties of ZnSe/p-Si Diode. *Politek Derg*. 2019, 22(1): 63-67.

[39] K. Ngai, S. Ramesh, K. Ramesh, J. Juan. A Review of Polymer Electrolytes: Fundamental, Approaches and Applications. Ionics (Kiel). 2016, 22(8): 1259-1279.

[40] T. Itoh, Y. Ichikawa, T. Uno, M. Kubo, O. Yamamoto. Composite Polymer Electrolytes Based on Poly (ethylene oxide), Hyperbranched Polymer, $BaTiO_3$ and $LiN(CF_3SO_2)_2$. *Solid State Ionics*. 2003, 156(3): 393-399.

[41] K. Praveenkumar, T. Sankarappa, J. Ashwajeet, R. Ramanna. Dielectric and AC conductivity studies in PPy-Ag nanocomposites. *J. of Polymers*. 2015(3): 1-5.

[42] Karar Abdali, Shireen R., Ali J. Mechanical Ultrasonic Properties of (Polymethylene Oxide-TiO_2) Polymer Composite Gel. *Journal of Engineering and Applied Sciences*. 2019, 14(3): 6002-6005.

[43] I. Sondi, B. Salopek-Sondi. Silver nanoparticles as antimicrobial agent: a case study on E. coli as a model for Gram-neg-ative bacteria. *Journal of Colloid and Interface Science*. 2014, 275(1): 177-182.

[44] Q. Cheng, A. Benozir, Y. Liu, Y. Peng, D. Diaz, Z. Shi, Z. Cui, R. Narain. Antifouling and Antibacterial Polymer-Coated Surfaces Based on the Combined Effect of Zwitterions and the Natural Borneol. ACS Appl. Mater. *Interfaces*. 2022, 13(7): 9006-9014.

[45] P. Badica, N. Batalu, M. Burdusel, M. Grigoroscuta, G. Aldica, M. Enculescu, G. Gradisteanu, M. Popa, L. Marutescu, B. Dumitriu, L. Olariu, A. Bicu, B. Purcareanu, L. Operti, V. Bonino, A. Agostino, M. Truccato, M. Chifiriuc. Antibacterial composite coatings of MgB_2 powders embedded in PVP matrix. *Scientific reports*. 2021, 11(1): 9591.

[46] H. Yu, X. Xiaoyi, X. Chen, T. Lu. Preparation and antibacterial effects of PVA-PVP hydrogels containing silver nanoparticles. *Journal of Applied Polymer Science*. 2007, 103(1): 125-133.

[47] Jehan A., Zainab A., Hamsa A. Antibacterial effect and structural properties of PVA-PVP-Ag nanocomposites. *Ejbps*. 2016, 3: 35-41.

[48] Y. Nho, Y. Lim, H. Gwon, E. Choi. Preparation and characterization of PVA/PVP/glycerin/antibacterial agent hydrogels using γ-irradiation followed by freeze-thawing. *Korean J. Chem. Eng*. 2009, 26(6): 1675-1678.

[49] M. Abd El-Kader, M. Elabbasy, A. Adeboye, A. Menazea.

Nanocomposite of PVA/PVP blend incorporated by copper oxide nanoparticles via nanosecond laser ablation for antibacterial activity enhancement. *Polymer Bulletin*. 2021, 5: 3975.

[50] E. Doğan, P. Tokcan, M. Diken, B. Yilmaz, B. Kizilduman, P. Sabaz. Synthesis, Characterization and Some Biological Properties of PVA/PVP/PN Hydrogel Nanocomposites: Antibacterial and Biocompatibility. *Advances in materials science*. 2019, 19: 32-45.